Geocarto International

ISSN: (Print) (Online) Journal homepage: https://www.tandfonline.com/loi/tgei20

Delineation of structural lineaments of the Southwest Sub-basin (East Vietnam Sea) using global marine gravity model from CryoSat-2 and Jason-1 satellites

Luan Thanh Pham, Saulo P. Oliveira, Minh Huy Le, Phan Trong Trinh, Tich Van Vu, Van-Hao Duong, To-Nhu Thi Ngo, Thanh Duc Do, Tho Huu Nguyen & Ahmed M. Eldosouky

To cite this article: Luan Thanh Pham, Saulo P. Oliveira, Minh Huy Le, Phan Trong Trinh, Tich Van Vu, Van-Hao Duong, To-Nhu Thi Ngo, Thanh Duc Do, Tho Huu Nguyen & Ahmed M. Eldosouky (2021): Delineation of structural lineaments of the Southwest Sub-basin (East Vietnam Sea) using global marine gravity model from CryoSat-2 and Jason-1 satellites, Geocarto International, DOI: 10.1080/10106049.2021.1981463

To link to this article: https://doi.org/10.1080/10106049.2021.1981463

Published online: 24 Sep 2021.

GEOCARTO INTERNATIONAL
https://doi.org/10.1080/10106049.2021.1981463

Taylor & Francis
Taylor & Francis Group

Delineation of structural lineaments of the Southwest Sub-basin (East Vietnam Sea) using global marine gravity model from CryoSat-2 and Jason-1 satellites

Luan Thanh Pham[a], Saulo P. Oliveira[b], Minh Huy Le[c], Phan Trong Trinh[d,e], Tich Van Vu[f], Van-Hao Duong[g], To-Nhu Thi Ngo[a], Thanh Duc Do[a], Tho Huu Nguyen[a] and Ahmed M. Eldosouky[h]

[a]Faculty of Physics, University of Science, Vietnam National University, Hanoi, Viet Nam; [b]Department of Mathematics, Federal University of Paraná, Curitiba, PR, Brazil; [c]Institute of Geophysics, Vietnam Academy of Science and Technology, Hanoi, Viet Nam; [d]Institute of Geological Sciences, Vietnam Academy of Science and Technology, Hanoi, Viet Nam; [e]Royal Academy for Overseas Sciences, Brussels, Belgium; [f]Faculty of Geology, University of Science, Vietnam National University, Hanoi, Viet Nam; [g]Hanoi University of Mining and Geology, Hanoi, Viet Nam; [h]Faculty of Science, Geology Department, Suez University, Suez, Egypt

ABSTRACT

In recent years, the analysis of satellite gravity data is used as a powerful tool for geologic mapping. This study is based on various filtered maps of Bouguer gravity anomaly data of the Southwest Sub-basin (East Vietnam Sea) to delineate its main structural lineaments. The effectiveness of modern filtering methods such as normalized analytical signal, improved version of tilt angle and enhanced horizontal gradient amplitude has been estimated with synthetic gravity anomalies before applying to the gravity data of the Southwest Sub-basin. For synthetic examples, the results show that the enhanced horizontal gradient amplitude not only provides edges with high resolution but also prevents spurious edges in the output maps. For real case, the obtained structural map is consistent with many faults already recognized in the Sub-basin, and the results provide new information leading to a better understanding of the structural framework and tectonic setting of the area.

ARTICLE HISTORY
Received 21 March 2021
Accepted 10 September 2021

KEYWORDS
Southwest Sub-basin; lineaments; gravity; CryoSat-2; Jason-1

1. Introduction

The knowledge of the lateral boundaries of subsurface structures in oceanic areas is of crucial interest in many geoscience applications, as the shapes of the structures, rather than their depths, are representative of the tectonic situation and history of these areas. The subsurface geologic structures can be determined by interpreting satellite gravity data, as well as other geophysical data. The gravimetric data have signals with a large dynamic amplitude range that depend on the geometry, depth and density of the source. Edge enhancing filters usually try to emphasize characteristics of the gravity field facilitating

CONTACT Luan Thanh Pham luanpt@hus.edu.vn

interpretation of geologic structures of gravimetric anomaly data (Pham, Vu, et al. 2020). There are many edge detectors based on gravity data derivatives for highlighting the source edges (Pham 2020a). Some edge detector techniques such as the gradient amplitude (Cordell and Grauch 1985), total gradient (Roest et al. 1992), enhanced total gradient (Hsu et al. 1996), are often used to extract the source boundaries, but their results are dominated by the signals generated by shallow structures (Nguyen et al. 2017; Pham, Oksum, Do, et al. 2021; Pham, Oksum, Le, et al. 2021; Pham, Oksum, Vu, et al. 2021). To balance the different signals, various techniques have been developed such as the tilt derivative (Miller and Singh 1994), the gradient amplitude of the tilt derivative (Verduzco et al. 2004), theta (Wijns et al. 2005), normalized horizontal derivative (Cooper and Cowan 2006). However, these filters tend to generate secondary boundaries in the edge maps (Pham, Oksum, Le, et al. 2021). Several approaches have been proposed to avoid this problem, such as the tilt derivative of the gradient amplitude (Ferreira et al. 2013), the normalized total gradient (Ma et al. 2015), the improved theta method (Yuan et al. 2016), the improved enhanced tilt derivative (Nasuti et al. 2019), the total directional theta method (Zareie and Moghadam 2019). Recently, Pham, Eldosouky, et al. (2020) have been developed another balanced filter extracting the edges, called the enhanced horizontal gradient amplitude filter, and proved that this filter is more effective than the traditional filters (i.e. total gradient, tilt derivative, the gradient amplitude of the tilt derivative theta, normalized horizontal derivative and tilt derivative of the gradient amplitude) in outlining the source horizontal boundaries. The use of edge enhancing filters has shown great success in extracting the lateral boundaries of the subsurface structures in the oceanic area (Pal et al. 2016; Narayan et al. 2017; Kha et al. 2018; Pham, Le, et al. 2018).

The East Vietnam Sea (also known as the South China Sea) is located at the junction of the Pacific Plate, Eurasian Plate and Indo-Australian Plate and is the key region of interaction between the Tethyan and Pacific tectonic domain (Li et al. 2012; Ding and Li 2016). With abundant mineral resources, especially, oil and natural gas (Zhang et al. 2012; Savva et al. 2014), its structural framework and tectonic setting have always been a significant research topic in Earth science community (Wang et al. 2020). The East Vietnam Sea can be divided into the East, Northwest and Southwest Sub-basins (Yu et al. 2018; Wang et al. 2020). Of these Sub-basins, the Southwest Sub-basin is the most important tectonic unit in the East Vietnam Sea (Ding and Li 2016). The study area extends from latitude 10°N to 12°N and longitude 111°E to 113°E (Figure 1). It is a critical exploration area in regard to the history of evolution of the East Vietnam Sea (Zhang et al. 2012). Previous gravity studies in the area were only focused on estimating the depths to density interfaces through inversion of gravity data. For example, Braitenberg et al. (2006), Dung et al. (2019) and Nguyen et al. (2020) determined the basement structures from the satellite-derived gravity data, while Li et al. (2010) estimated the depth to the Moho interface from simple Bouguer gravity data. Li et al. (2008) and Yu et al. (2017) applied the gradient amplitude and total gradient methods to magnetic data to extract the structural lineaments of the East Vietnam Sea. However, the results obtained from these methods are dominated by large amplitude anomalies. In addition, since their study covers a very large area, their map of estimated lineaments in the area is of low resolution. Guo et al. (2015) used the hybrid positive-and-negative curvature method for detection of the edges of magnetic anomalies in the East Vietnam Sea. Although the edges can be determined by the zero contours of the hybrid curvature, it generates spurious zero contours around sources, making it difficult to interpret the geological structures. Some other authors (e.g. Gao et al. 2009; Ding et al. 2016; Ding and Li 2016; Zhang et al. 2019) used

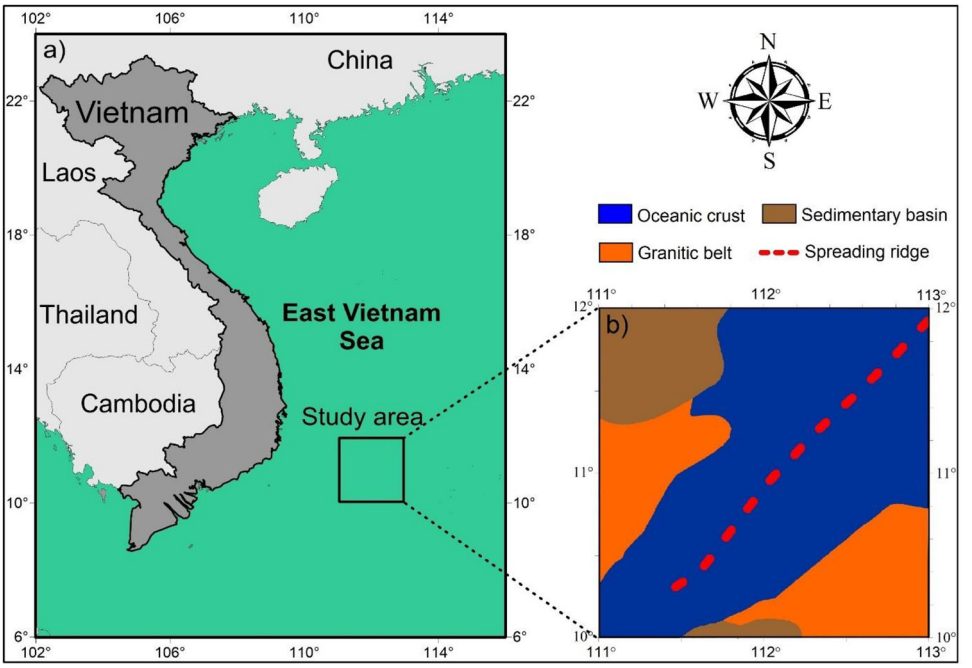

Figure 1. (a) Location of the study area and (b) tectonic map of the area (modified from Savva et al. 2014).

multichannel seismic data to study structures along some cross-sections of the Southwest Sub-basin.

This study has two major objectives viz., (1) estimation of the effectiveness of advanced filtering methods such as normalized analytical signal (NAS), improved version of tilt angle and enhanced horizontal gradient amplitude using 3D models, (2) applying these methods to the gravity data derived from the CryoSat-2 and Jason-1 satellites to delineate structural lineaments of the Southwest Sub-basin (East Vietnam Sea). The results obtained from this work provide a better understanding of the advanced processing filters, also new elements which allow for improving knowledge on the structure of the Southwest Sub-basin.

2. Geological setting

The East Vietnam Sea is one of the largest marginal seas in the western Pacific, which was formed as a result of the continental margin rifting and spreading started $\sim$ 65 Ma ago (Taylor and Hayes 1983; Pichot et al. 2014). It is bounded to the north by the South China continental margin, to the south by Truong Sa islands block, to the east by the Indochina block and to the west by the Philippine block. The East Vietnam Sea has a complex tectonic history with abundant natural resources, especially, hydrocarbon (gas and oil; Zhang et al. 2012).

Two opposite kinematic models of opening the East Vietnam Sea represent two mechanisms that involve distinct driving forces. In the first model, the opening of the East Vietnam Sea is only driven by the inferred sub-duction of the older oceanic crust into the North Borneo trough to the south (Taylor and Hayes 1980). In the second model, the continental rift is first developed at the tip of propagating left-lateral strike-slip faults. The extension is then driven by the relative motion of Indochina and then pushed towards the

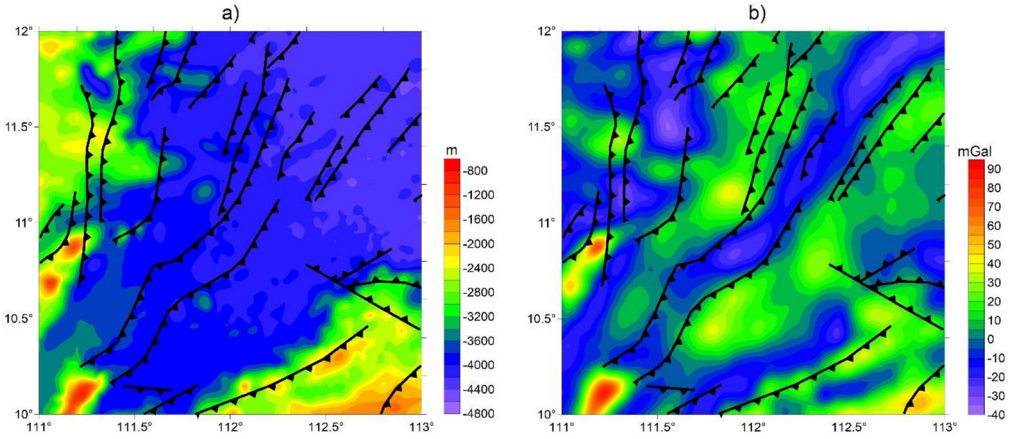

Figure 2. (a) Bathymetry map and (b) free-air gravity anomaly of the study area. The black lines show the faults in the study region (Gao et al. 2009).

SE relative to South China by the penetration of India into Asia (Tapponnier et al. 1982; Leloup et al. 1995). Seafloor spreading in the East Vietnam Sea took place between 32 and 15 Ma. During the latest Oligocene, the spreading axis jumped to the south and propagated south-westward throughout the Early Miocene (Briais et al. 1993). Some studies on lateral extrusion have addressed the Red River and Qui Nhon basins located at the northern part of the Phu Khanh Basin, which was formed through left-lateral strike-slip displacement across the East Vietnam Boundary Fault Zone (Leloup et al. 1995).

Some studies on lateral extrusion have addressed the Red River and Qui Nhon basins located at the northern part of the Phu Khanh Basin, which was formed through left-lateral strike-slip displacement across the East Vietnam Boundary Fault Zone (Leloup et al. 1995). In the studied region, following a ridge start at around 25 Ma, the Southwest Sub-basin with NE-strike started to open and the spreading terminated at 16 Ma. The age of the oceanic crust in the SW Sub-basin was interpreted principally according to the magnetic anomaly (Briais et al. 1993). Although non-similar dating and locating were introduced, the oceanic crust gets younger from east to west due to the multiphased opening of a graben and NE trending basin developed along the continental shelf (Huang et al. 2019; Dong et al. 2020).

Based on bathymetric topography and magnetic anomaly characteristics, the East Vietnam Sea is commonly divided into three Sub-basins: the East, Northwest and Southwest Sub-basins (Wang et al. 2020). Our study corresponds to the Southwest Sub-basin, which is located in the southwestern region of the East Vietnam Sea. Figure 2(a) shows the bathymetry map (Smith and Sandwell 1997) of the Southwest Sub-basin with many NE-SW trending faults that controlled the basin formation (Gao et al. 2009). The bathymetry data was obtained from global sea floor topography (Smith and Sandwell 1997; Sandwell et al. 2014), which is derived from satellite altimetry and ship depth soundings. The data is available from Scripps Institution of Oceanography (University of California San Diego, United States) for download at https://topex.ucsd.edu/cgi-bin/get_data.cgi. This Sub-basin is a V-shaped Sub-basin opening to the northeast, and its average water depth is about 4000 m (Figure 2(a)). It is characterized by NE-SW tectonic trends (Li et al. 2012). Recent studies show that seafloor spreading in the Southwest Sub-basin started around 23.6 Ma and stopped around 16 Ma (Li et al. 2014; Yu et al. 2018; Wang et al. 2020), which is consistent with the spreading age model reported by Taylor and Hayes

(1983) and Briais et al. (1993). The model of Li et al. (2014) suggests that the Southwest Sub-basin is a slow spreading ridge with the spreading rate decreased from 50 to 35 km/Myr at the end of expansion in the East Vietnam Sea. In contrast to the East Vietnam Sea, the analysis of magnetic anomalies in the Southwest Sub-basin shows shallower Curie depths with an average depth of 27 km and higher heat flow with an average value of 120 mW/m^2, indicating a younger oceanic crust (Li et al. 2010). The results obtained from interpreting multichannels seismic data show that the depth to the basement in the study area ranges from 2.5 to 5 km (Lu et al. 2016), while the depth calculated from gravity data ranges from 4.0 to 6.5 km (Nguyen et al. 2020). The reason is that Nguyen et al. (2020) used the Parker-Oldenburg method (Oldenburg 1974) that is based on the assumption that the density of sedimentary rocks above the basement interface is uniform. However, the density of sediments is rarely uniform in nature, so this assumption is often unrealistic (Chakravarthi et al. 2013; Pham, Oksum, et al. 2018).

3. Data and methodology

3.1. Data

The gravity data set used in this study is based on $1' \times 1'$ grid gravity data derived from the CryoSat-2 and Jason-1 satellites, which has two times more accuracy compared to the previous gravity model (Figure 2(b); Sandwell et al. 2014). To obtain the Bouguer gravity anomaly, the gravitational effect of seawater is replaced with the gravitational effect of rock using a density contrast of 1.64 g/cm^3. After the correction, the Bouguer gravity map of the study area is shown in Figure 2(b) (Pham 2020a, 2020b). In recent years, the applications of the boundary enhancement techniques to the satellite gravity data have shown great success (Vaish and Pal 2015; Pal et al. 2016; Kumar et al. 2018, 2020; Kunnummal and Anand 2019; Pham et al. 2019; Chouhan et al. 2020; Pham, Kafadar, et al. 2021).

3.2. Methodology

One of the classical applications of gravimetric methods is the detection of subsurface geologic structures. This section describes the theoretical background of the modern filtering methods such as NAS, improved version of tilt angle and enhanced horizontal gradient amplitude.

The NAS, introduced by Ma (2015), normalizes the gradient amplitude of the analytical signal using the absolute value of the vertical derivative of the analytical signal. The method is given by:

$$\mathrm{NAS} = \operatorname{atan} \frac{\sqrt{\left(\frac{\partial \mathrm{AS}}{\partial x}\right)^2 + \left(\frac{\partial \mathrm{AS}}{\partial y}\right)^2}}{\left|\frac{\partial \mathrm{AS}}{\partial z}\right|}, \tag{1}$$

where ∂AS/∂x, ∂AS/∂y and ∂AS/∂z are the x, y and z derivatives of the AS, respectively. The AS is given by:

$$\mathrm{AS} = \sqrt{\left(\frac{\partial F}{\partial x}\right)^2 + \left(\frac{\partial F}{\partial y}\right)^2 + \left(\frac{\partial F}{\partial z}\right)^2}, \tag{2}$$

where $\partial F/\partial x$, $\partial F/\partial y$ and $\partial F/\partial z$ are the derivatives of the potential field data F. The source horizontal boundaries are determined by the maximum values of NAS.

Nasuti et al. (2019) proposed the HG_STDR filter which uses a combination of the second-order vertical gradient and the derivatives of the horizontal gradient. The peaks of HG_STDR can be used to extract the source edges. The HG_STDR method is given by:

$$\mathrm{HG_{STDR}} = \sqrt{\left(\frac{\partial \mathrm{STDR}}{\partial x}\right)^2 + \left(\frac{\partial \mathrm{STDR}}{\partial y}\right)^2}, \tag{3}$$

where STDR is defined as

$$\mathrm{STDR} = \mathrm{atan}\frac{M \times \frac{\partial^2 F}{\partial z^2}}{\sqrt{\left(\frac{\partial \mathrm{HGA}}{\partial x}\right)^2 + \left(\frac{\partial \mathrm{HGA}}{\partial y}\right)^2}} \tag{4}$$

with M is absolute gravity value of the study area, $\partial^2 F/\partial z^2$ is the second-order vertical derivative of the field F, $\partial \mathrm{HGA}/\partial x$ and $\partial \mathrm{HGA}/\partial y$ are the x and y gradients of the HGA that is and given by

$$\mathrm{HGA} = \sqrt{\left(\frac{\partial F}{\partial x}\right)^2 + \left(\frac{\partial F}{\partial y}\right)^2}. \tag{5}$$

Another filter for enhancing the edge of the magnetic and gravity sources is introduced by Pham, Eldosouky, et al. (2020) which is based on the inverse sine function and the ratio between the vertical to the total gradient of the horizontal gradient amplitude HGA. The filter is given by:

$$\mathrm{EHGA} = \mathcal{R}\left(a\sin\left(k\left(\frac{\frac{\partial \mathrm{HGA}}{\partial z}}{\sqrt{\left(\frac{\partial \mathrm{HGA}}{\partial x}\right)^2 + \left(\frac{\partial \mathrm{HGA}}{\partial y}\right)^2 + \left(\frac{\partial \mathrm{HGA}}{\partial z}\right)^2}} - 1\right) + 1\right)\right), \tag{6}$$

where k is a positive real number which is decided by the interpreter, $\partial \mathrm{HGA}/\partial z$ is z gradient of the HGA. The EHGA generates the maximum amplitudes on the source horizontal boundaries. In general, the k value greater than or equal to 2 will bring the best results. Due to the nature of the inverse sine function, the EHGA values vary from $-\pi/2$ to $+\pi/2$. We have implemented the above filters as scripts for use in the software MATLAB, version R2017a or above.

4. Synthetic model study

The effectiveness of the advanced processing methods is tested with gravity examples that includes six prismatic sources with parameters given in Table 1. Figure 3(a,b) show the 3D and plan views of the model. The gravity anomaly of the model was calculated at 201×201 grid nodes with 1 km spacing using Rao et al. (1990) method (Figure 4(a)).

Table 1. The parameters of the synthetic model.

Parameters/Sources	1	2	3	4	5	6
Centre coordinates (km; km)	70; 100	70; 100	70; 100	145; 125	145; 75	175; 100
Width (km)	30	50	90	25	25	4
Length (km)	30	50	90	25	25	140
Depth of top (km)	1	2	5	1	2.5	1
Depth of bottom (km)	2	5	8	2.5	4	3
Density contrast (g/cm^3)	−0.1	0.1	0.2	−0.3	−0.3	−0.3

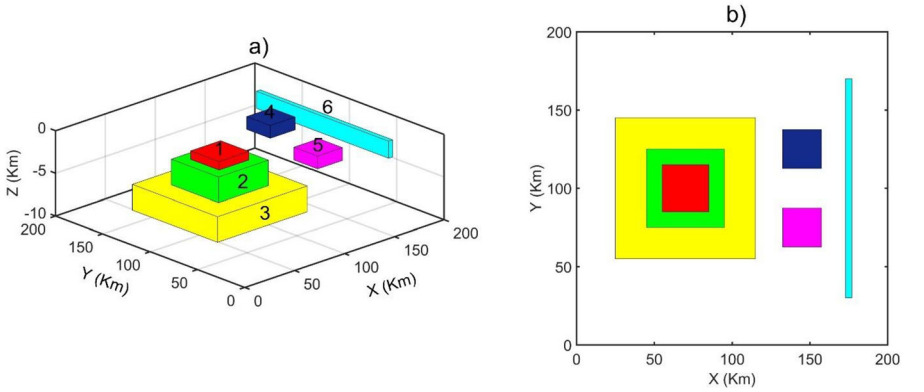

Figure 3. Three dimensional and plan views of the synthetic model.

Figure 4(b) shows the NAS map. As it can be seen, the NAS method is very effective in equalizing the signals with the different amplitudes. This method can detect the edges of the source 1, but for other sources, the peaks of the NAS are shifted out from the true borders, making estimated edges appear larger than reality. In addition, the NAS method produces the secondary boundaries around the sources 1 and 2, and above the sources 4 and 5. Figure 4(c) shows the HG_STDR map. Clearly, the HG_STDR filter allows for a more accurate estimation of the source edges compared to the NAS filter. Although this method shows a very high resolution for the estimated edges, it brings the secondary edges above the source 1 and around the sources 2, 4 and 5. Figure 4(c) shows the EHGA map with the estimated edges are located over the source edges. Similar to the HG_STDR method, the EHGA method also provides an image with high resolution. However, the EHGA method can avoid producing the secondary edges around or above the sources.

To examine the performance of the methods in noisy case, the gravity data in Figure 4(a) was corrupted with 5% Gaussian noise. The noise-corrupted data is displayed in Figure 5(a). Figure 5(b,c) depict the edge maps detected by applying the NAS and HG_STDR methods, respectively. Although the HG_STDR method produces more accurate results than the NAS method, both methods are strongly affected by the noise in the data, and these methods also produce secondary boundaries in the input maps. Figure 5(d) displays the edges estimated by the EHGA method. We can see that the method is less sensitive to noise than other methods. The method provides the edges with high resolution, and it does not bring any false information.

As the methods use second derivatives of the gravity data, it is recommended to apply an upward continuation filter to noisy data before calculation of the edges. In Figure 6(a), an upward continuation filter of 1 km was applied to the noisy data from Figure 5(a). Here, a trial-and-error procedure has been used to detect the height of the upward continuation of the gravity data. Figure 6(b,c,d) depict the edges determined by the NAS, HG_STDR and EHGA methods, respectively. Although the HG_STDR method yields more accurate edges compared to the NAS filter, both methods bring the false boundaries in the input maps. In this case, the EHGA map shows the edges more clearly than other methods. Moreover, the EHGA is less sensitive to noise than the NAS and HG_STDR methods, and there is not any misleading information in the EHGA edge map.

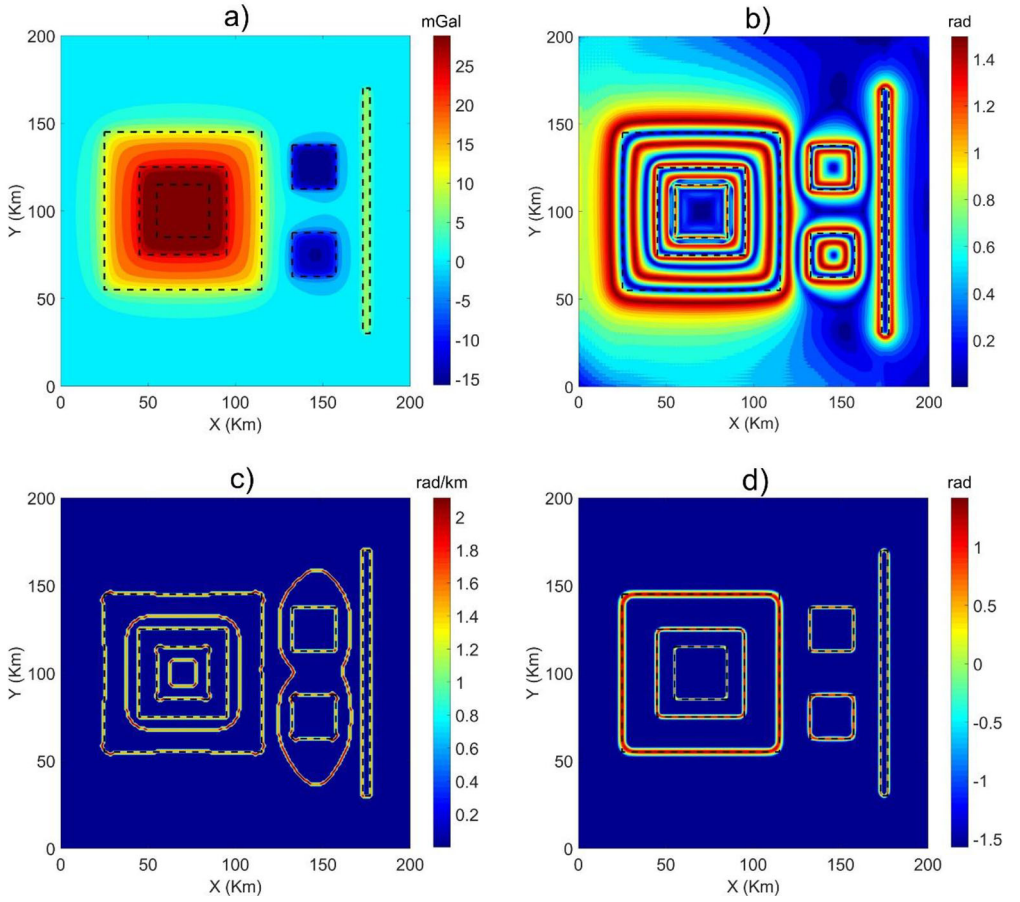

Figure 4. (a) Gravity anomaly without noise, (b) NAS, (c) HG_STDR and (d) EHGA.

5. Results of application to gravity data of the Southwest Sub-basin

The Bouguer gravity data (Figure 7(a)) used in this study was computed by Pham (2020b) using $1' \times 1'$ grid gravity data derived from the CryoSat-2 and Jason-1 satellites. The result determined by applying the NAS method is shown in Figure 7(b). This method is effective in balancing the large and small signals. However, the NAS method yields the results with lower resolution, and some adjacent boundaries are connected, making it difficult to extract geological structures. Figure 7(c) shows the result determined by using the HG_STDR method. Although this filter provides the higher resolution results compared to the NAS method, some adjacent boundaries determined by this method are also connected. Moreover, as shown in the model examples, both the NAS and HG_STDR methods give rise to artifacts in the edge detection results. Thus, using the results from the NAS and HG_STDR methods may lead to wrong interpretations of the structures of the area. Figure 7(d) shows the result of applying the EHGA method to the Bouguer gravity anomaly data in Figure 7(a). We can see that the EHGA filter can show the gravity lineaments more clearly compared to other methods. Clearly, the method not only equalizes the weak and strong anomalies simultaneously but also avoids connecting the adjacent boundaries.

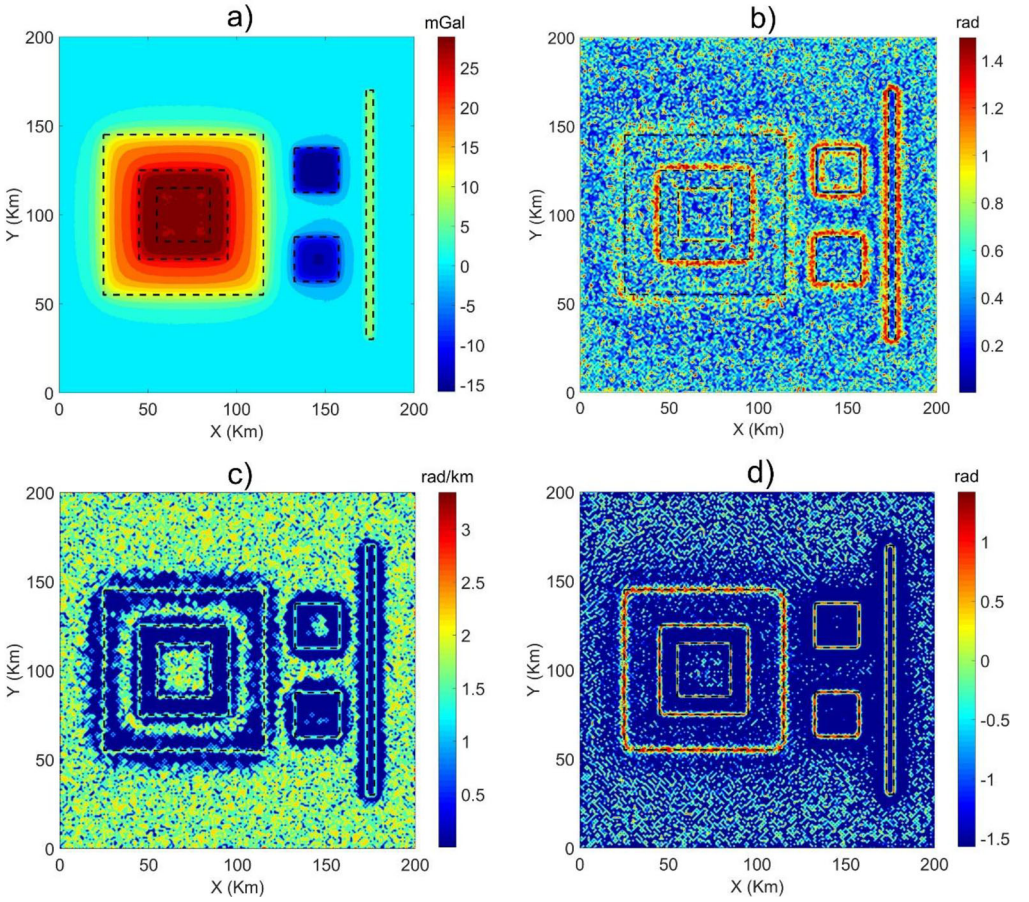

Figure 5. (a) Gravity anomaly with noise, (b) NAS, (c) HG_STDR and (d) EHGA.

According to Jacobsen (1987) and Kebede et al. (2020), when the gravity field is upward continued to a height z, it maps the sources located at and below the depth $z/2$. The results obtained from interpreting multichannels seismic data show that the depth to the basement in the study area ranges from 2.5 to 5 km (Lu et al. 2016). Thus, an upward continuation of 5 km was applied to the Bouguer gravity data in order to reduce the noise effect and aid extraction of structures buried at and below the depths 2.5 km (Figure 8(a)). Figure 8(b,c,d) shows the result estimated by the NAS, HG_STDR and EHGA methods, respectively. The edge map determined from application of the NAS method once again shows that the NAS does not function well for extracting the gravity lineaments. The NAS method is also more sensitive to noise than the HG_STDR and EHGA methods, and the lineaments obtained from this method are more diffuse than those extracted from other filters. Like the above results, the boundaries extracted by the NAS and HG_STDR methods appear to be more interconnected, complicating the detection of geological structures. It is worth noting the HG_STDR and EHGA methods can determine the edges in higher resolution compared to the NAS filter. However, the EHGA map shows the lineaments more clearly compared to the NAS and HG_STDR maps.

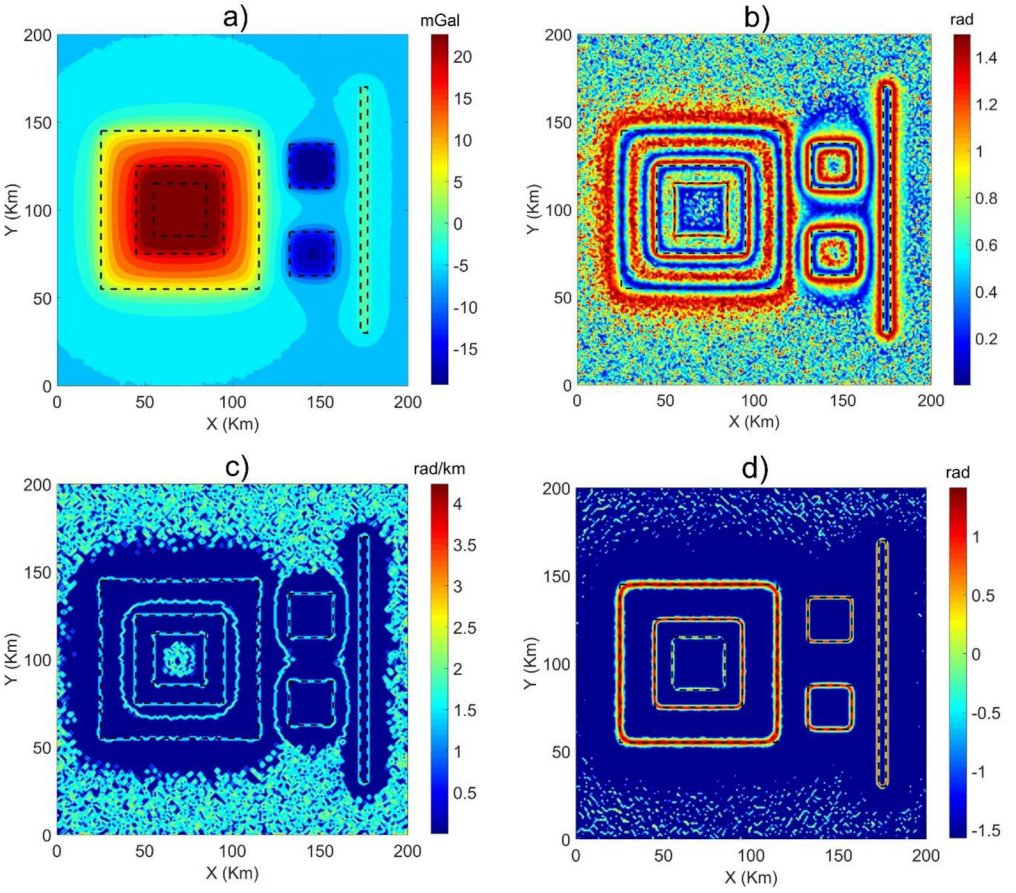

Figure 6. (a) Upward continued gravity anomaly, (b) NAS, (c) HG_STDR and (d) EHGA.

6. Discussions

A comparison of the results obtained from the synthetic examples (Figures 4–6) shows that the EHGA method detects the edges of all sources much better than the NAS and HG_STDR methods. In the NAS method, the found edges are more than in reality. In addition, the edges detected by this method appear more diffuse and wider than they are. Unlike the NAS method, the HG_STDR method extracts the edges of causative bodies with very high accuracy with any diffused boundaries. However, it is noteworthy that both the NAS and HG_STDR methods yield the false edges that tend to connect. Figures 4(d), 5(d) and 6(d) show that the EHGA method can provide reliable results even for gravity field due to multiple interfering sources. Another advantage of the EHGA method is that it is less sensitive to noise than the NAS and HG_STDR methods. The reason is that the NAS is based on the derivatives of the analytic signal, and the HG_STDR method uses third-order derivatives, whereas the EHGA method uses only the first-order derivatives of the horizontal gradient (Pham et al. 2019).

The NAS, HG_STDR and EHGA methods are also applied to the gravity data from the Southwest Sub-basin (East Vietnam Sea). In the NAS method, the ratio between the derivatives of analytical signal is used to balance the signals with the different amplitudes. However, as shown in Figures 7(b) and 8(b), the differentiation of the analytical signal

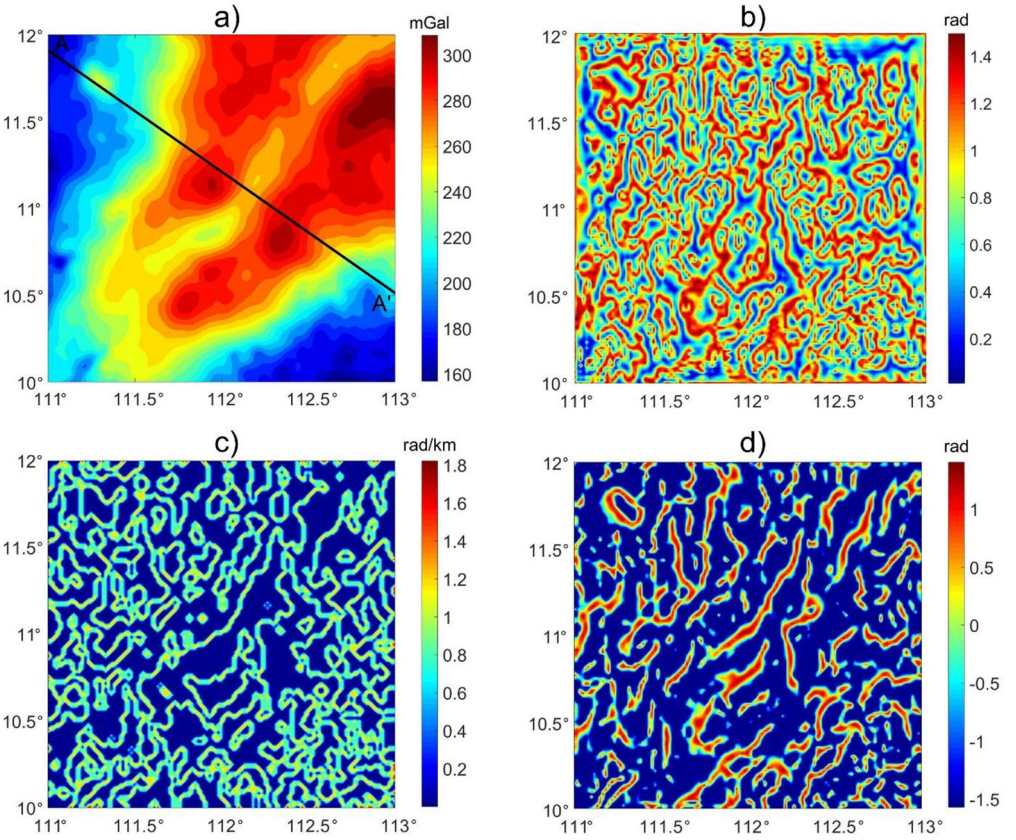

Figure 7. (a) Bouguer gravity anomaly, (b) NAS, (c) HG_STDR and (d) EHGA. Black line in (a) shows the location of the seismic section presented in the following.

might amplify the noisy signals, which is one of the main disadvantages of the NAS method. In addition, as we showed in the synthetic model, the NAS method does not exactly define the source edges. For real case, the peaks of the NAS do not show the same trends with the faults already recognized in the Sub-basin (Figure 2). These peaks also do not match with the contacts between the known geological units in the area (Figure 1(b)). Because the zero contours of the second-order vertical derivative of the gravity anomaly data are near the edges of the density structures, the HG_STDR method can bring a more accurate estimation of the source horizontal boundaries. The results obtained from this method (Figures 7(c) and 8(c)) show a good correlation with the NE-SW trend of geology structures in the area (Figures 1(b) and 2). Unfortunately, the HG_STDR method produces some false structures. The reason is that the second-order vertical derivative also produces the false zero contours around the sources. These false zero contours tend to connect, making it difficult to delineate geological structures. It is known that any true geological lineament is continuous for some distance until terminated at another lineament, which would be a fault or contact (Tschirhart and Morris 2015). In this case, the edges estimated by the EHGA method are oriented in the same trend (Figures 7(d) and 8(d)). The peaks of the EHGA correspond to the horizontal boundaries of buried structures. Hence, they enable to extract the lineaments/faults in the Southwest Sub-basin. By comparing estimated structures by the EHGA method with the known geologic structures (Figure 1(b)), we can see that the contacts between Oceanic crust and other geologic

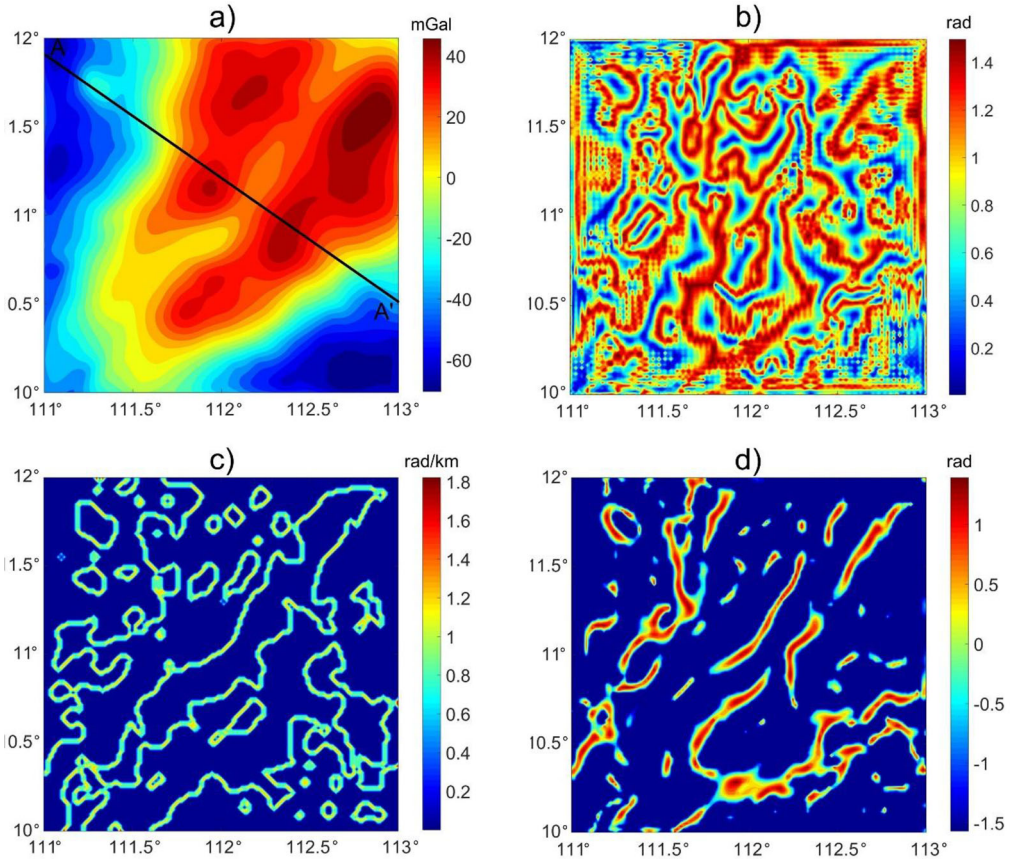

Figure 8. (a) Upward continued Bouguer gravity anomaly, (b) NAS, (c) HG_STDR and (d) EHGA. Black line in (a) shows the location of the seismic section presented in the following.

formation types are well extracted by the EHGA method. In general, the lineaments in the EHGA maps correlate very well with the geologic characteristics in the Southwest Sub-basin. For another comparison, Figure 9(b) shows the EHGA values of the Bouguer gravity data and upward continued Bouguer gravity data (Figure 9(a)) along the cross-section AA′ which the seismic data of this section has been interpreted by PetroVietnam (Figure 9(c)). It can be seen that there is a good correlation between seismic data and the images of the EHGA, with many of peaks indicating the faults.

The boundary detection results of the EHGA method in Figures 7(d) and 8(d) are marked to locate the lineaments and corresponding strike directions. The rose diagrams of the marked lineaments using the EHGA filter show a major trend in NE-SW direction (Figure 10(c,d)). We compare in Figure 10(a,b) the density boundaries interpreted from the EHGA maps with the faults reported by Gao et al. (2009). We can see that the NE-SW trending lineaments in the EHGA maps show a good correlation with the trend of the known normal faults in the Southwest Sub-basin. The faults controlled the Sub-basin formation are also of NE-SW trend and formed grabens mostly (Gao et al. 2009). The EHGA maps illustrate the presence of NE-SW directed faults characterized by an extensional movement which is responsible for the partition of the region into blocks. The existence of these faults indicates strong extensional tectonic activity that resulted in the formation of several half-grabens and domino-style rotated blocks, as reported by Ding et

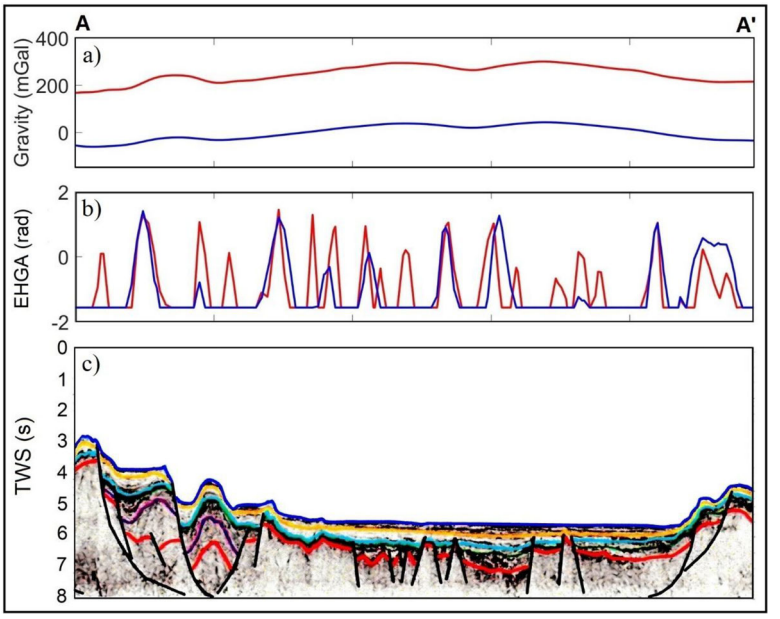

Figure 9. (a) Bouguer gravity data (red line) and upward continued Bouguer gravity data (blue line) of the profile shown in Figures 7(a) and 8(a). (b) EHGA of Bouguer gravity data (red line) and EHGA of upward continued Bouguer gravity data (blue line) and (c) interpreted seismic section.

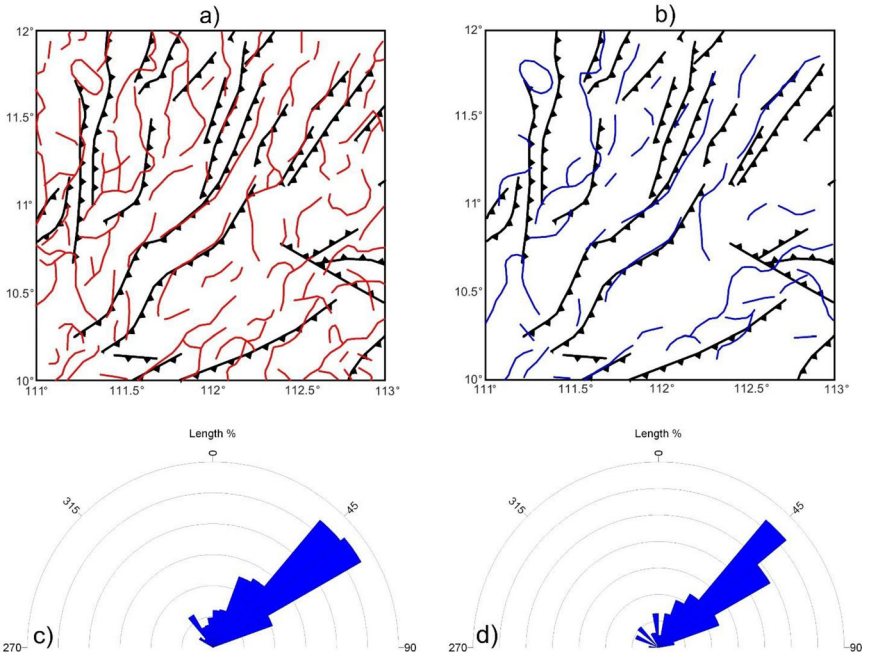

Figure 10. (a) Superposition of the lineaments extracted by the EHGA of the Bouguer gravity data with faults reported by Gao et al. (2009). (b) Superposition of the lineaments extracted by the EHGA of the upward continued gravity data at a height of 5 km with faults reported by Gao et al. (2009), (c) synoptic rose diagram representing marked lineament/faults trends of the Bouguer gravity data and (d) synoptic rose diagram representing marked lineament/faults trends of the upward continued gravity data.

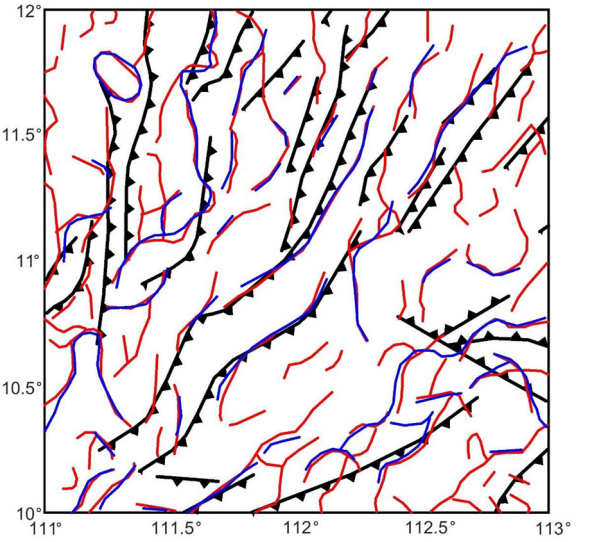

Figure 11. Superposition of the lineaments extracted by the EHGA maps of the Bouguer gravity data with faults reported by Gao et al. (2009).

al. (2016). Various models for the opening of the East Vietnam Sea were proposed. The first considered the collision between India and Eurasia directed to the extrusion of the Indochina and the opening of the East Vietnam Sea (Tapponnier et al. 1982; Leloup et al. 1995). Other models suggested a mantle plume was at the origin of the extension (Flower et al. 1998). The third model proposed dragging of the Proto-East Vietnam Sea subduction resulted in the extension and formation of the East Vietnam Sea (Taylor and Hayes 1983). Although the models are different, they accepted the extension along the Southwest Sub-basin with NE-strike.

Figure 11 shows the superposition of the lineaments obtained from application of the EHGA filter to the Bouguer gravity data and upward continued gravity data at a height of 5 km. We can see that the lineaments of the upward-continued data are more continuous, which may reflect deep structures. The obtained results in Figure 11 compare favorably with the V-shaped configuration of the Southwest Sub-basin. The existence of the NE-SW trending lineaments in the EHGA maps indicates that the Sub-basin appears to extend farther northeast beyond the border of the interpreted map, which is also well reflected in the rifting model in the SWSB of Ding et al. (2016) and Ding and Li (2016). Moreover, some lineaments coincide with NE-SW trending faults defined by the analysis of the reflection seismic data (Ding and Li 2016). In addition, the results obtained from the EHGA filter demonstrate the existence of many lineaments that are not extracted by other geophysical/geological studies. For example, the circular one at the northwest corner, or the long ones around latitude 10.5°N and longitude 112°E to 112.5°E. These results illustrate the usefulness of the EHGA method for interpreting gravity data. The EHGA filter balances the amplitudes of the anomalies generated by shallow and deep structures, making the most of the information existed in gravity data, for interpretation of qualitative research.

7. Conclusions

We considered the effectiveness of modern filtering methods such as NAS, HG_STDR and EHGA in geologic mapping through gravity data. Initially, the gravity anomalies of

the synthetic model with and without noise have been enhanced using these methods. Findings show that the structures detected by the NAS are larger than reality, both NAS and HG_STDR methods produce the secondary boundaries in the edge maps, whereas the EHGA filter allows for an accurate estimation of the source edges without any false edges. Further, the NAS, HG_STDR and EHGA have been applied to gravity data of the Southwest Sub-basin (East Vietnam Sea) to delineate its main structural lineaments. The obtained results show that the lineaments of all wavelengths have been enhanced by using these methods. However, the NAS method yields the results with lower resolution, and the lineaments extracted by the NAS and HG_STDR methods are connected, making it difficult to extract geologic structures. The results also reveal that the EHGA method could be regarded as more suitable density lineament delineation method than the NAS and HG_STDR methods. It is observed from the EHGA maps that the lineaments show a major trend in NE-SW direction, which compare favourably with many faults already recognized in the Southwest Sub-basin. Moreover, the results obtained from this study show the existence of many new structures that are not determined by other geophysical/geological studies.

Disclosure statement

No potential conflict of interest was reported by the author(s).

Data availability statement

Data available on request from the authors.

References

Briais A, Patriat P, Tapponnier P. 1993. Updated interpretation of magnetic anomalies and seafoor spreading stages in the South China Sea: implications for the tertiary tectonics of Southeast Asia. J Geophys Res. 98(B4):6299–6328.

Braitenberg C, Wienecke S, Wang Y. 2006. Basement structures from satellite-derived gravity field: South China Sea ridge. J Geophys Res. 111(B5):B05407.

Chakravarthi V, Sastry SR, Ramamma B. 2013. MODTOHAFSD – A GUI based JAVA code for gravity analysis of strike limited sedimentary basins by means of growing bodies with exponential density contrast–depth variation: a space domain approach. Comput Geosci. 56:131–141.

Chouhan AK, Singh D, Pal SK, Choudhury P. 2020. Delineation of subsurface geological fractures in the Cambay rift and surrounding regions of NW India: an integrated approach using satellite derived EIGEN-6C4 gravity data. Geocarto Int. 1–16. doi:10.1080/10106049.2020.1716395.

Cooper GRJ, Cowan DR. 2006. Enhancing potential field data using filters based on the local phase. Comput Geosci. 32(10):1585–1591.

Cordell L, Grauch VJS. 1985. Mapping basement magnetization zones from aeromagnetic data in the San Juan Basin, New Mexico. In: Hinze WJ, editor. The utility of regional gravity and magnetic maps. 1st ed. Tulsa: Society of Exploration Geophysicists; p. 181–197.

Ding W, Li J. 2016. Propagated rifting in the Southwest Sub-basin, South China Sea: insights from analogue modelling. J Geodyn. 100:71–86.

Ding W, Li J, Clift PD. 2016. Spreading dynamics and sedimentary process of the Southwest Sub-basin, South China Sea: constraints from multi-channel seismic data and IODP Expedition 349. J Asian Earth Sci. 115:97–113.

Dong M, Wu S, Zhang J, Xu X, Gao J, Song T. 2020. Lithospheric structure of the Southwest South China Sea: implications for rifting and extension. Int Geol Rev. 62(7-8):924–937.

Dung TT, Kulinich RG, Sang NV, Que BC, Dai NB, Dung NK, Dung TT, Lap TT. 2019. Improving accuracy of altimeter-derived marine gravity anomalies for geological structure research in the Vietnam South-Central continental shelf and adjacent areas. Russ J Pac Geol. 13(4):364–374.

Ferreira FJF, de Souza J, de Bongiolo ABeS, de Castro LG. 2013. Enhancement of the total horizontal gradient of magnetic anomalies using the tilt angle. Geophysics. 78(3):J33–J41.
Flower MFJ, Tamaki K, Hoang N. 1998. Mantle extrusion: a model for dispersed volcanism and DUPAL-like asthenosphere in East Asia and the Western Pacific. In: Flower MFJ, Chung SL, Lo CH, Lee TY, editors. Mantle dynamics and plate interactions in East Asia. Geodynamics Series. Vol. 27; p. 67–88. Washington, D.C., American Geophysical Union.
Gao H, Zhou D, Qiu Y. 2009. Relationship between formation of Zhongyebei basin and spreading of southwest subbasin, South China Sea. J Earth Sci. 20(1):66–76.
Guo L, Gao R, Meng X, Zhang G. 2015. A hybrid positive-and-negative curvature approach for detection of the edges of magnetic anomalies, and its application in the South China Sea. Pure Appl Geophys. 172(10):2701–2710.
Huang H, Qiu X, Pichot T, Klingelhoefer F, Zhao M, Wang P, Hao T. 2019. Seismic structure of the Northwestern margin of the South China Sea: implication for asymmetric continental extension. Geophys J Int. 218(2):1246–1261.
Hsu SK, Sibuet JC, Shyu CT. 1996. High-resolution detection of geologic boundaries from potential field anomalies: an enhanced analytic signal technique. Geophysics. 61(2):373–1957.
Jacobsen BH. 1987. A case for upward continuation as a standard separation filter for potential-field maps. Geophysics. 52(8):1138–1148.
Kebede H, Alemu A, Fisseha S. 2020. Upward continuation and polynomial trend analysis as a gravity data decomposition, case study at Ziway-Shala basin, central Main Ethiopian rift. Heliyon. 6(1):e03292.
Kha VT, Vuong VH, Thanh DD, Hung QD, Anh DL. 2018. Improving a maximum horizontal gradient algorithm to determine geological body boundaries and fault systems based on gravity data. J Appl Geophys. 152:161–166.
Kumar U, Pal SK, Sahoo SD, Narayan S, Saurabh MS, Ganguli SS. 2018. Lineament mapping over sir creek offshore and its surroundings using high resolution EGM2008 gravity data: an integrated derivative approach. J Geol Soc India. 91(6):671–678.
Kumar S, Pal SK, Guha A, Sahoo SD, Mukherjee A. 2020. New insights on Kimberlite emplacement around the Bundelkhand Craton using integrated satellite-based remote sensing, gravity and magnetic data. Geocarto Int. 1–23. doi:10.1080/10106049.2020.1756459.
Kunnummal P, Anand SP. 2019. Qualitative appraisal of high resolution satellite derived free air gravity anomalies over the Maldive Ridge and adjoining Ocean Basins, Western Indian Ocean. J Asian Earth Sci. 169:199–209.
Leloup P, Lacassin R, Tapponnier P, Scharer U, Zhong D, Liu X, Zhang L, Ji S, Trinh PT. 1995. The Ailao Shan-Red River shear zone (Yunnan, China), Tertiarytransform boundary of Indochina. Tectonophysics. 251(1-4):3–84.
Li CF, Zhou Z, Li J, Chen B, Geng J. 2008. Magnetic zoning and seismic structure of the South China Sea ocean basin. Mar Geophys Res. 29(4):223–238.
Li C-F, Shi X, Zhou Z, Li J, Geng J, Chen B. 2010. Depths to the magnetic layer bottom in the South China Sea area and their tectonic implications. Geophys J Int. 182(3):1229–1247.
Li JB, Ding WW, Wu ZY, Zhang J, Dong CZ. 2012. The propagation of seafloor spreading in the Southwest Sub-basin, South China Sea. Chin Sci Bull. 57(20):1896–1905.
Li CF, Xu X, Lin J, Sun Z, Zhu J, Yao YJ, Zhao XX, Liu QS, Kulhanek DK, Wang J, et al. 2014. Ages and magnetic structures of the South China Sea constrained by deep tow magnetic surveys and IODP Expeition 349. Geochem Geophys Geosyst. 15(12):4958–4983.
Lu C, Hao T, Yao Y, Xing J, Qiu X. 2016. Oceanic mantle gravimetric response to the seafloor spreading of the Southwest Sub-basin, South China Sea. Geol J. 51:535–547.
Ma G, Liu C, Huang D. 2015. The removal of additional edges in the edge detection of potential field data. J Appl Geophys. 114:168–173.
Miller HG, Singh V. 1994. Potential field tilt a new concept for location of potential field sources. J Appl Geophys. 32(2-3):213–217.
Narayan S, Sahoo SD, Pal SK, Kumar U, Pathak VK, Majumdar TJ, Chouhan A. 2017. Delineation of structural features over a part of the Bay of Bengal using total and balanced horizontal derivative techniques. Geocarto Int. 32(4):351–366.
Nasuti Y, Nasuti A, Moghadas D. 2019. STDR: a novel approach for enhancing and edge detection of potential field data. Pure Appl Geophys. 176(2):827–841.
Nguyen TN, Van Kha T, Van Nam B, Nguyen HTT. 2020. Sedimentary basement structure of the Southwest Sub-basin of the East Vietnam Sea by 3D direct gravity inversion. Mar Geophys Res. 41(1):7.
Nguyen HTT, Do TD, Le MH. 2017. Application of directional derivative method to determine boundary of magnetic sources by total magnetic anomalies. Vietnam J Earth Sci. 39(4):360–375.

Oldenburg DW. 1974. The inversion and interpretation of gravity anomalies. Geophysics. 39 (4):526–536.
Pal SK, Narayan S, Majumdar TJ, Kumar U. 2016. Structural mapping over the 85°E Ridge and surroundings using EIGEN6C4 high-resolution global combined gravity field model: an integrated approach. Mar Geophys Res. 37(3):159–184.
Pichot T, Delescluse M, Chamot-Rooke N, Pubellier M, Qiu Y, Meresse F, Sun G, Savva D, Wong KP, Watremez L, et al. 2014. Deep crustal structure of the conjugate margins of the SW South China Sea from wide-angle refraction seismic data. Mar Pet Geol. 58:627–643.
Pham LT, Le MH, Oksum E, Do TD. 2018. Determination of maximum tilt angle from analytic signal amplitude of magnetic data by the curvature-based method. Vietnam J Earth Sci. 40(4):354–366.
Pham LT, Oksum E, Do TD. 2018. GCH_gravinv: a MATLAB-based program for inverting gravity anomalies over sedimentary basins. Comput Geosci. 120:40–47.
Pham LT, Oksum E, Do TD. 2019. Edge enhancement of potential field data using the logistic function and the total horizontal gradient. Acta Geod Geophys. 54(1):143–155.
Pham LT. 2020a. A comparative study on different filters for enhancing potential field source boundaries: synthetic examples and a case study from the Song Hong Trough (Vietnam). Arab J Geosci. 13(15): 723.
Pham LT. 2020b. A comparative study on different methods for calculating gravity effect of an uneven layer: application to computation of Bouguer gravity anomaly in the East Vietnam Sea and adjacent areas. VNU J Sci Math Phys. 36(3):106–114.
Pham LT, Vu TV, Le-Thi S, Trinh PT. 2020. Enhancement of potential field source boundaries using an improved logistic fiter. Pure Appl Geophys. 177(11):5237–5249.
Pham LT, Eldosouky AM, Oksum E, Saada SA. 2020. A new high resolution filter for source edge detection of potential field data. Geocarto Int. 1–18. doi:10.1080/10106049.2020.1849414.
Pham LT, Oksum E, Vu MD, Vo QT, Le-Viet KD, Eldosouky AM. 2021. An improved approach for detecting ridge locations to interpret the potential field data for more accurate structural mapping: a case study from Vredefort dome area (South Africa). J Afr Earth Sci. 175:104099.
Pham LT, Oksum E, Le DV, Ferreira FJF, Le ST. 2021. Edge detection of potential field sources using the softsign function. Geocarto Int. 1–14. doi: 10.1080/10106049.2021.1882007.
Pham LT, Oksum E, Do TD, Nguyen DV, Eldosouky AM. 2021. On the performance of phase-based filters for enhancing lateral boundaries of magnetic and gravity sources: a case study of the Seattle Uplift. Arab J Geosci. 14(2):129.
Pham LT, Kafadar O, Oksum E, Eldosouky AM. 2021. An improved approach for detecting the locations of the maxima in interpreting potential field data. Arab J Geosci. 14(1):43.
Rao DB, Prakash MJ, Ramesh Babu N. 1990. 3-D and 2 1/2-D modeling of gravity anomalies with variable density contrast. Geophys Prospect. 38(4):411–422.
Roest WR, Verhoef J, Pilkington M. 1992. Magnetic interpretation using the 3-D analytic signal. Geophysics. 57(1):116–125.
Sandwell DT, Müller RD, Smith WHF, Garcia E, Francis R. 2014. New global marine gravity model from CryoSat-2 and Jason-1 reveals buried tectonic structure. Science. 346(6205):65–67.
Savva D, Pubellier M, Franke D, Chamot-Rooke N, Meresse F, Steuer S, Auxietre JL. 2014. Different expressions of rifting on the South China Sea margins. Mar Pet Geol. 58:579–598.
Smith WHF, Sandwell DT. 1997. Global seafloor topography from satellite altimetry and ship depth soundings. Science. 277(5334):1956–1962.
Tapponnier P, Peltzer G, Le Dai AY, Armijo R, Cobbold P. 1982. Propagatingextrusion tectonics in Asia: new insights from simple experiments with plasticine. Geology. 10(12):611–616.
Taylor B, Hayes DE. 1980. The tectonic evolution of the South China Basin. In: Hayes DE, editor. The tectonic and geologic evolution of Southeast Asian Seas and Islands, Part 1, Geophys. Monogr. Set. 23. Washington, DC: AGU; p. 89–104.
Taylor B, Hayes DE. 1983. Origin and history of the South China Sea basin. In: Hayes DE, editor. The tectonic and geologic evolution of Southeast Asian Seas and Islands. Washington, DC: American Geophysical Union; p. 23–56.
Tschirhart P, Morris B. 2015. Improved edge detection mapping through stacking and integration: a case study in the Bathurst Mining Camp. Geophys Prospect. 63(2):283–295.
Vaish J, Pal SK. 2015. Geological mapping of Jharia Coalfield, India using GRACE EGM2008 gravity data: a vertical derivative approach. Geocarto Int. 30(4):388–401.
Verduzco B, Fairhead JD, Green CM, MacKenzie C. 2004. New insights into magnetic derivatives for structural mapping. Leading Edge. 23(2):116–119.

Wang Q, Zhao M, Zhang H, Zhang J, He E, Yuan Y, Qiu X. 2020. Crustal velocity structure of the Northwest Sub-basin of the South China Sea based on seismic data reprocessing. Sci China Earth Sci. 63(11):1–16.

Wijns C, Perez C, Kowalczyk P. 2005. Theta map: edge detection in magnetic data. Geophysics. 70(4): L39–L43.

Yu X, Xue C, Shi H, Zhu W, Liu Y, Yin H. 2017. Expansion of the South China Sea basin: constraints from magnetic anomaly stripes, sea floor topography, satellite gravity and submarine geothermics. Geosci Front. 8(1):151–162.

Yu J, Yan P, Wang Y, Zhang J, Qiu Y, Pubellier M, Delescluse M. 2018. Seismic evidence for tectonically dominated seafloor spreading in the Southwest Sub-basin of the South China Sea. Geochem Geophys Geosyst. 19(9):3459–3477.

Yuan Y, Gao JY, Chen LN. 2016. Advantages of horizontal directional Theta method to detect the edges of full tensor gravity gradient data. J Appl Geophys. 130:53–61.

Zareie V, Moghadam RH. 2019. The application of theta method to potential field gradient tensor data for edge detection of complex geological structures. Pure Appl Geophys. 176(11):4983–5001.

Zhang Z, Du Y, Gao L, Fang N, Yang S, Liu J, Song C. 2012. The late mesozoic granodiorites from the southwest basin in the South China Sea and its tectonic implication. J Earth Sci. 23(3):268–276.

Zhang J, Chen J, Huang Y. 2019. Moho structure of the Southwest Sub-basin, South China Sea, from a multichannel seismic reflection profile NH973-1. J Ocean Univ China. 18(5):1105–1110.